



Dynamic Forced Impingement Cooling: Latest Experimental Results Regarding Variations in Flow Guidance and Pulse Parameters

Frank Haucke^(✉), Arne Berthold, and Niklas Meyners

Department of Aeronautics and Astronautics, Chair of Aerodynamics,
Technische Universität Berlin, Marchstr. 12–14, 10587 Berlin, Germany
{frank.haucke.1, arne.berthold}@tu-berlin.de,
niklas.meyners@campus.tu-berlin.de
https://www.sfb1029.tu-berlin.de/menu/sfb_1029/

Abstract. Convective heat transfer of a hot surface in a regime of a periodically pulsed 7 by 7 cooling air impingement jet array is experimentally investigated. In the category of geometrical parameters wall curvature was added. Based on a flat target plate configuration two additional wall curvatures for impingement jet flow guidance were focused on to enhance geometrical boundary conditions in style of real turbine blades. Thereby, internal structure of pressure and suction side is represented by a convex and a concave shaped impingement jet flow space with the same constant radius. For all three experimental configurations nozzle and impingement distance were kept constant at three nozzle diameters. Convective heat transfer behaviour achieved for flat plate setup is transferable for both additional investigated curvatures. The dynamic parameters, frequency, phase shift and duty cycle, separately as well as combined have a significant influence on convective heat transfer improvements compared to the corresponding steady blowing case.

Keywords: Heat transfer · Experimental · Impingement cooling · Periodic forcing · Pulsed blowing · Phase shift · Duty cycle · Crossflow · Wall curvature

1 Introduction

The efficiency of modern gas turbines has increased over the last few decades constantly, which has led to a turbine inlet temperature of more than 1600 K [1]. The increased turbine inlet temperature is one main method for the efficiency gain, while the other one is a raised turbine pressure ratio. In order to reach such high temperatures, several improvements to the maximum permitted thermal material load are needed, which are achieved by the use of thermal barrier coatings, the development of super temperature resistant alloys as well as the convective cooling of turbine blades via internal and external mechanisms.

In order to further increase the efficiency of gas turbines, either the maximum allowed temperature of the turbine blade material needs to be increased or the cooling mechanisms of the blades need to be improved.

Internal steady blowing impingement cooling is an already implemented concept, which features a higher local heat transfer coefficient in comparison to classical convective cooling inside of the turbine blade. The improved cooling efficiency achieved by this concept is applied on the inner surface, where the cooling air mass flow impinges as jets before being channelled through the blade and exiting it at the trailing edge. Due to this flow, a crossflow interacting with downstream jets is created. To improve this cooling concept, several geometric parameters have been determined as important by Florschuetz et al. [2,3], Weigand and Spring [4] and Xing et al. [5]. These parameters include the nozzle diameter, nozzle arrangement, nozzle distance, impingement distance and the Reynolds number of the cooling air mass flow. An improvement to this concept is dynamically forced impingement cooling, which features the generation of strong vortex structures leading to an increased local convective heat transfer in comparison to the steady blowing method. It was shown by Liu and Vejrazka [6,7] using a single forced impingement jet that the heat transfer in the wall jet region is affected by a dynamically forced impingement jet without significantly influencing the stagnation zone. The distance to the impingement plate H/D has been determined as a driving parameter. Since this improvement is achieved by the vortex structures, the interaction of these vortices in an array of impinging jets is of particular interest for an increased gain of cooling efficiency.

These results were confirmed by Hofmann et al. [8], who showed that the main reason for the change in heat transfer depending on the nozzle to impingement plate distance H/D is the mixing effect of the jets with the environment due to their interaction. Depending on the impingement distance, the mean jet velocity and therefore the heat transfer on the target plate is reduced by the mixing effects. This effect is larger the longer the impingement distance is. A possible increase of the heat transfer due to the turbulence magnitude and the Strouhal number of the dynamically forced jets being of the same order was found by Hoffman, which led to a threshold Strouhal number of $Sr_D = 0.2$ [8]. A formation number $t^* = \frac{(u_p \cdot t)}{D}$ describing the generation of high-energy ring vortices in dependency of the nozzle diameter D , the nozzle exit velocity u_p and the process time t was defined by Gharib et al. from 1998 [9]. This formation number and the threshold Strouhal number were linked by Janetzke [10] which in turn links the works of Herwig et al. [11], Middleberg et al. [12] and Janetzke et al. [10] to the limits for the generation of ring vortices with maximized vorticity, size and amplitude found by Gharib. These works describe the use of velocity square wave signals to produce strong vortices by which strong temporal and local velocity gradients are created which lead to a maximized local convective heat transfer. The local Nusselt numbers increase and the combination of amplitude and frequency are dependent on each other while also being influenced by system resonance and other actuator characteristics which further underlines the

importance of an detailed investigation of the connection of local heat transfer in the wall jet and stagnation zone and the dynamically forced impinging jets.

To further increase the cooling ratio the additional parameters duty cycle and phase shift between adjacent nozzle should be considered. In the field of flow control it was shown that flow stability is enhanced while the control mass flow is reduced due to a reduction of the duty cycle at constant maximum jet exit velocity [13]. It was shown by Scholz et al. [14] that duty cycles as low as $DC = 25\%$ are increasing normal force coefficient very effectively. Furthermore it was stated by the authors that a high potential for flow conditioning lies in the optimization of the duty cycle. Even though both studies were focused on jets for separation control, the findings are also applicable for impingement cooling. The momentum coefficient c_μ of a jet in a pulsed flow regime with a constant mass flow rate and a square wave form is proportional to $\frac{1}{DC}$ [15]. This correlation together with the increased temporal velocity leads to the generation of strong vortex structures. In the application of impingement cooling the wall shear stress is increased by the increased local and temporal wall gradients induced by the vortices generated by the jets. Since convective heat transfer is directly linked to the wall shear stress, the duty cycle is most likely a driving parameter for further optimization of the impingement cooling concept. The phase shift between adjacent nozzles can be used to optimize the vortex ring interaction and therefore potentially increasing the cooling ratio even further.

The present experimental investigation is focused on the local convective heat transfer under a 7 by 7 dynamically forced impinging jet array with side-wall induced crossflow. In comparison to previous investigations the nozzle spacing is reduced to $S/D = 3$, which causes stronger jet interactions. As a new geometrical parameter wall curvature was included in this experimental investigation. Based on a flat target plate configuration two additional wall curvatures for impingement jet flow guidance were focused on enhancing the geometrical boundary conditions in style of real turbine blades. Thereby, internal structure of pressure and suction side is represented by a convex and a concave shaped impingement jet flow space. In detail, the study focuses on the local convective heat transfer for several combinations of the excitation frequency, the phase shift between adjacent rows of nozzles, the duty cycle and the nozzle Reynolds number. Thereby, the focus is on maximization of the local convective heat transfer.

2 Experimental Setup

The following section contains information regarding the experimental setup. The basic testing configuration was already utilized by previously conducted work [16–21]. Convective heat transfer between an electrically heated wall and a set of interacting dynamically forced impingement jets is investigated. Figure 1 illustrates the current experimental setup of this work. The geometric impinging jet pattern is produced by jet nozzles arranged in a standard inline 7 (N_X) by 7 (N_Y) array with a reduced dimensionless spacing of $S/D = 3$ in the main directions of the X-Y plane. The nozzle X-locations are defined as follows:

$$\frac{X}{D}(n_X) = \left(n_X - \frac{1}{2} \cdot (N_X + 1) \right) \cdot \frac{S_X}{D} \quad (1)$$

This nozzle plate is positioned above the target plate in various distances ($Z/D = H/D = 2, 3, 5$). Three corresponding side walls, one upstream at $X_{wall}/D = -3.5 \cdot S_X/D$ and two at $Y_{wall}/D = \pm 3.5 \cdot S_Y/D$, border the flow space laterally and define the resulting crossflow in positive x direction. The coordinate origin is located at the intersection of the central longitudinal nozzle axis with the target plate. The inner nozzle geometry is equivalent as utilized in previous work [16–21] and is based on the geometry introduced by Janetzke [10]. Thus, the average crossflow Reynolds number Re_{CF} is increased with every row of impingement nozzles until a maximum is generated shortly upstream of the last row. This kind of crossflow generation is derived from a turbine blade, where the internal structure is channelling the exploited cooling mass flow to the trailing edge of the turbine blade. With every nozzle row the mean Reynolds number ratio of crossflow (CF) and nozzle jet (D) increases and follows the simplified equation:

$$\frac{Re_{CF}}{Re_D}(n_X) = \frac{\bar{U}_{CF}(n_X) \cdot H}{\bar{U}_D \cdot D} \cdot \frac{\nu_D}{\nu_{CF}} \approx \frac{\pi}{4} \cdot \frac{n_X - 1}{S_Y/D} \quad (2)$$

Furthermore, wall curvature was considered in this work as a new geometrical parameter taken into account for enhancing experimental boundary conditions towards more realistic flow topology. Therefore, in addition to the standard flat target plate setup two more experimental setups were investigated, one with a convex and another one with a concave curved impingement plate flow space (see Fig. 1). These 2D curvatures represent structural conditions of internally cooled parts in style of turbine blades. The wall curvature radius was derived from NASA E^3 profile shape [22, 23]. The realistic radius was upscaled and matched to the generic nozzle diameter employed in this work. Both curved setups have the same radius but with convex and concave shaped target plates representing inner walls, one on the pressure side and the other one on the suction side of turbine blade. Thereby, the experimental focus lies on the curvature driven influence on wall jet propagation and the resulting convective wall heat transfer. With introducing 2D wall curvature nozzle axes of adjacent rows are inclined due to the perpendicular alignment to the target plate. Within every row nozzle axes remain parallel. Apart from this all test setups are basically equivalent.

The coolant air mass flow is provided by an in house compressed air system. Based on the experimental configuration seven individual mass flow control units (MFCU) were utilized. With an accuracy of 0.1–0.5% each of them feeds a set of seven nozzle jets in each row, located at a constant crossflow position, see Fig. 2. This connection technique combined with a symmetric air flow divider (not displayed) enables the cooling air mass flow to be distributed as evenly as possible among the nozzles in each row, particularly in the case of non-coherent actuation.

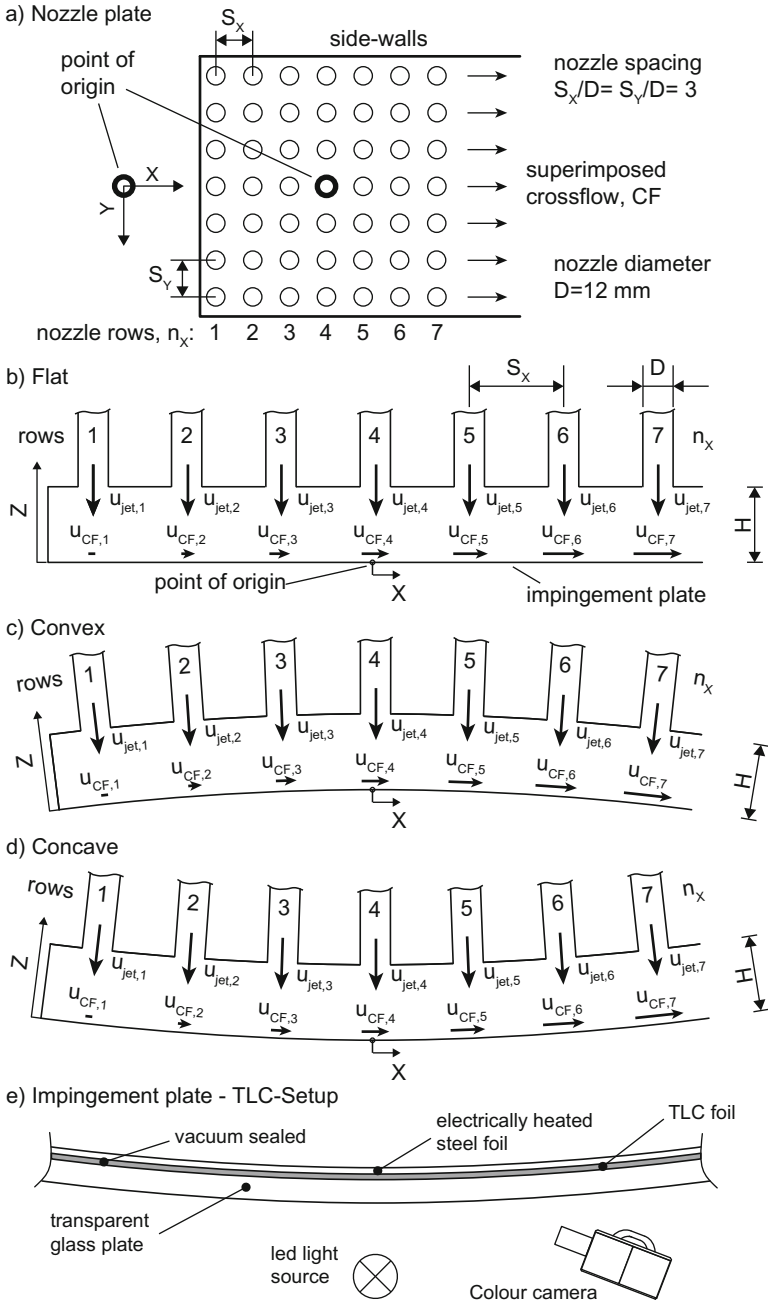


Fig. 1. a) Bottom view of nozzle plate with schematic nozzle arrangement, X , Y plane at $Z = H$, $S/D = H/D = 3$. b-d) Side views of crossflow mid sections, X , Z plane at $Y = 0$, $Z > 0$: b) Flat configuration, c) Convex configuration, d) Concave configuration. e) Impingement plate with TLC-setup.

The dynamic deformation of impinging jets was enabled by employing an individual fast switching solenoid valve in front of every single nozzle. Thereby, the maximum pulse frequency and maximum normalized volume flow rate are limited at $f_{max} = 1000\text{ Hz}$ and $V_N \leq 160\text{ l}_N/\text{min}$ by the utilized solenoid valves. Based on these specifications, switching frequency was varied within the range of $f = 0$ to 1000 Hz at three nozzle exit based Reynolds numbers $Re_D = 3000, 5000, 7000$. Dynamic forced cases were compared to the corresponding steady blowing case in order to quantify the achieved benefit.

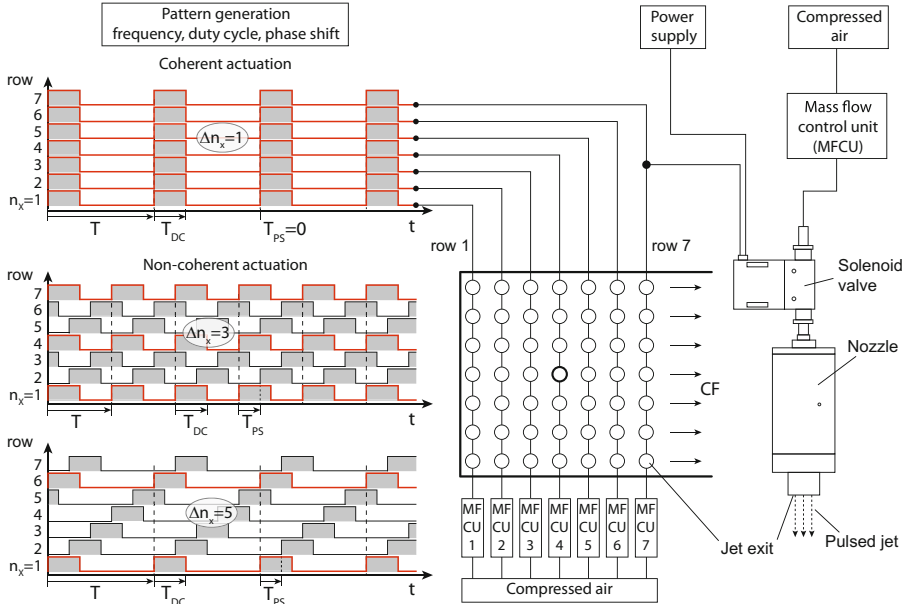


Fig. 2. Pulse pattern after start-up process, parameters and schematic presentation for dynamic control of impinging jets. Examples for coherent and non-coherent pulse patterns.

For these investigations each row was operated simultaneously with parameter variations based on frequency, duty cycle and phase-shift between adjacent rows. In this context, precise signal timing of each impingement jet pulse is a very fundamental part of this work. In order to meet the requirements for valve control most efficiently an Arduino microcontroller board was modified and programmed for multiple signal generation with a reference input square wave signal provided by a function generator. Thereby, pulse parameters can be set independently and are defined as followed.

Pulse frequency f (Hz) defines the temporal repetition of pulses of one jet and focuses primarily on the dynamic development of wall boundary layers in comparison to steady blowing case.

$$f = \frac{1}{T}, T - \text{periodic time in (s)} \quad (3)$$

In Fig. 2 different signal patterns are displayed exemplarily. For coherent actuation seven square wave signals are generated simultaneously or in phase. In case of non-coherent pulsation, pulse time shift defines the time delay between control signals of adjacent nozzle rows. It impacts temporal and spatial propagation of wall jets and boundary layer development compared to the coherent pulsed flow case. Due to the periodic property of each control signal defined by pulse frequency the period duration can be expressed by the following expressions:

$$PS = \frac{\Delta T_{PS}}{T} = \frac{1}{\Delta n_X}, \Delta T_{PS} - \text{pulse time shift in (s)} \quad (4)$$

$$T = \Delta n_X \cdot \Delta T_{PS}, \Delta n_X - \text{repetition number (-)} \quad (5)$$

The repetition number Δn_X is calculated by the reciprocal value of phase shift PS . If Δn_X , as a real number, takes an even value, it can be interpreted as a spatial interval between simultaneously switching valves in X direction, see Fig. 2. According to Eq. 4 a phase shift of $PS = 0\%$ is mathematically not allowed but it is equivalent to $PS = 100\%$ after the start-up process when all valves are switching. In this case Δn_X equals one, which means adjacent jets are pulsed coherently.

Duty cycle DC (%) defines the duration of jet pulse within one period, which follows in good approximation the square wave control signal for the valves.

$$DC = \frac{T_{DC}}{T}, T_{DC} - \text{pulse duration time in (s)} \quad (6)$$

The transfer behaviour of a square wave signal to a jet does not have to be one-to-one because it may be influenced by flow and geometry properties and have to be considered if necessary. Depending on the amount of mean cooling air mass flow or mean nozzle Reynolds number combined with geometry of air supply the jet properties such as exit velocity, amplitude, kinetic energy and momentum are defined. Thus, at a constant nozzle mass flow rate or nozzle Reynolds number a reduction of pulse duration ideally leads to a inversely proportional increase of jet momentum [15] (Eq. 7).

$$\dot{I}_D \approx \frac{1}{DC_D} \cdot \bar{m}_D \cdot \bar{U}_D \quad (7)$$

Due to the valves switched on and off a pulsated jet flow is generated. Thus, the mean momentum ratio between crossflow and impinging jet is driven by the pulse parameters discussed above and can be expressed by the simplified Eq. 8. Due to the incoming pulsed impinging jets the resulting crossflow underlies fluctuations as well. Since the jets impinge on the target plate directional fluctuations are dampened and deflected partly in crossflow direction but they are reduced to a minimum due to strong mixing interactions. Thus, the cross flow duty cycle DC_{CF} can be set to one in good approximation.

$$\frac{\dot{I}_{CF}}{\dot{I}_D}(n_X) \approx (n_X - 1)^2 \cdot \frac{\pi}{4} \cdot \frac{1}{S_Y/D \cdot H/D} \cdot \frac{DC_D}{DC_{CF}}, DC_{CF} \approx 1 \quad (8)$$

The structure of the heated impingement plate is illustrated in Fig. 1e). This version contains a 0.05 mm thin steel foil with the self-adhesive commercial thermochromic liquid crystal-film (TLC) attached to the reverse side. The film combination was vacuum sealed on a glass plate. Electrical power was used to generate wall heat flux using a power supply unit with $P_{max} = 3700$ W. This interacts directly with the attached TLC-foil resulting in a temperature distribution visible by LED illumination from the bottom side through the glass plate. Liquid crystals reflect temperature specific wave lengths of the illuminating light source and were captured by a colour camera. The electrical current through the steel foil was continuously controlled until temperature range defined by TLC-foil and a thermal equilibrium inside the test rig chamber was achieved for each operation point. Furthermore, each colour picture was de-warped and combined with the corresponding colour-calibration-matrix which results in the time averaged temperature distribution on the wall. More detailed information regarding the whole processing chain are contained in the work of Berthold et al. [20].

In order to evaluate convective heat transfer on the target zone induced by impinging jets some underlying assumptions need to be mentioned. It is postulated that the 3D heat flux into the structure is negligibly small compared to the heat transfer into the cooling air flow. Operating points are measured at a state of thermal equilibrium inside the whole test rig chamber. Thereby, the temperature gradient driven structural heat flux as well as radiation effects are minimized and are almost constant. In this context it is assumed that the thermal energy supplied by electrical power was transferred completely into the cooling air mass flow of the impinging jets which is expressed by the following Eq. 9 for Nusselt number calculation.

Based on the assumptions mentioned above Nusselt number can be expressed by the electrical Power P , the heated area A_{heat} , the balance between local wall and the nozzle jet temperature ($T_W - T_D$), the thermal conductivity of air λ_{air} and the nozzle diameter D . Due to the low Mach numbers ($Ma = 0.03$) the ratio between total and static temperature is nearly one ($T_{D0}/T_D \approx 1$).

$$Nu = \frac{\alpha \cdot D}{\lambda_{air}} = \frac{\dot{q}}{T_W - T_D} \cdot \frac{D}{\lambda_{air}} = \frac{P}{A_{heat} \cdot (T_W - T_D)} \cdot \frac{D}{\lambda_{air}} \quad (9)$$

Considering all possible measurement uncertainties, the overall theoretical uncertainty of the Nusselt number was determined as $\delta Nu/Nu = 3-8\%$. Nevertheless, reproducibility studies revealed an maximal experimental random uncertainty of 3%.

3 Experimental Results

In the following section results of experimental investigations are presented and discussed.

Flat Impingement Plate: In Fig. 3a) the reference 2D Nusselt number distribution on the flat plate configuration with a reduced nozzle spacing of $S/D = 3$ and an impingement distance of $H/D = 3$ at a steady blowing ($DC_D = 100\%$) nozzle Reynolds number of $Re_D = 7000$ is illustrated. The depicted Y/D range represents the mid section of the target zone in crossflow direction. Here, it is visible that the convective heat transfer is sufficiently symmetric to the centre line represented by $Y/D = 0$.

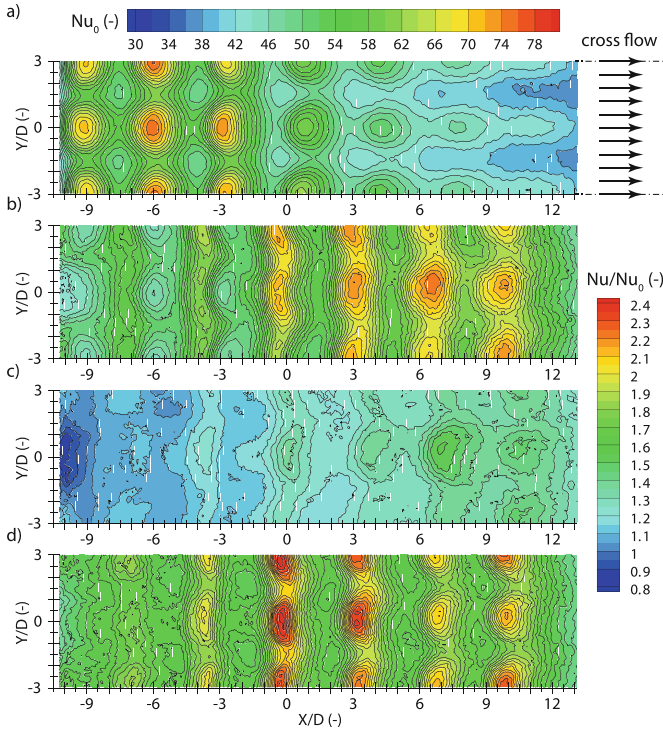


Fig. 3. Local convective heat transfer distributions for flat plate configuration with $S/D = 3$ and $H/D = 3$ at $Re_D = 7000$. a) Local absolute Nusselt numbers, steady blowing $DC_D = 100\%$. b–d) Local Nusselt number ratios, coherent pulsed blowing vs. steady blowing: b) $f = 300$ Hz, $DC_D = 50\%$, $PS = 0\%$, c) $f = 500$ Hz, $DC_D = 50\%$, $PS = 0\%$, d) $f = 800$ Hz, $DC_D = 50\%$, $PS = 0\%$.

Due to the blocked discharge upstream at $X/D = -10.5$ crossflow is generated in positive X/D direction. Thereby, the local crossflow component is accumulated by the discharge of upstream nozzle rows, see Eq. 2 and overlays the local impinging jets. Due to the increasing crossflow component in positive X/D direction the deflection of downstream impinging jets increases with every row which is visible by the increasing downstream shift of impinging zones with maximum local Nusselt numbers and the simultaneous deformation of the circular

jet shape. The contour plots b), c) and d) of Fig. 3 illustrate the distributed enhancement in convective heat transfer expressed by the local Nusselt numbers related to the steady blowing case Nu_0 for selected pulse frequencies. For $f = 300$ Hz and $f = 800$ Hz the local Nusselt number ratios are consequently larger than one ($Nu/Nu_0 > 1$) which indicates positive enhancements in convective heat transfer induced by pulsed blowing. Due to the larger temporal jet momentum in case of pulsed actuation the impinging jets can better penetrate the local crossflow which leads to significantly reduced deflection jet axes. Therefore, particularly high values of Nu/Nu_0 are located mainly in secondary flow areas outside local jet impingement zones of the steady blowing case. In picture c) of Fig. 3 the effect of coherent pulsed blowing on local convective heat transfer using a frequency of $f = 500$ Hz is illustrated. Thereby, Nusselt number ratios below one $Nu/Nu_0 \approx 0.88$ can be detected for $X/D < -8.5$ which corresponds to a reduction in heat transfer compared to the steady blowing case. In downstream direction $X/D > -8.5$ local enhancements can be achieved but they undercut by far the achievements of case b) and d).

In Fig. 4 extracted data from contour plots discussed above are displayed. Data curves represent the corresponding centre lines at $Y/D = 0$. In case of steady blowing local stagnation zones upstream of the centre nozzle match very good with their geometrical X/D positions ($n_X = 1, 2, 3$). This is also valid for pulsed cases $f = 500$ Hz and $f = 800$ Hz. Only marginal deviations are visible. In 300 Hz pulsed case stagnation zones for $n_X = 2$ and $n_X = 3$ are shifted even upstream from their geometrical position against local crossflow component more significantly. This indicates different outflow conditions for the local pulsed impinging jets and the accompanying generation of enclosing ring vortices and their propagation especially close to wall. Downstream of the centre nozzle ($n_X > 4$, $X/D > 0$) stagnation zone shift increases with every nozzle row and is most deviated for steady blowing while it is minimized for 800 Hz pulsed blowing case. Nusselt number ratios indicate that periodic actuation is capable of increasing convective heat transfer on the wall significantly almost everywhere on target plate but especially in the corresponding wall jet zones upstream of the stagnation areas of steady impingement jets.

Based on contour plots discussed above (Fig. 3) spatially averaged Nusselt number ratios were calculated and plotted versus pulse frequency. These results are displayed in Fig. 5. Additionally, experimental data of two more geometric flat plate configurations represented by $H/D = 2$ and $H/D = 5$ are inserted for equivalent pulse parameters. All Nusselt numbers are related to the corresponding steady blowing case. Pulse frequency with duty cycle of $DC_D = 50\%$ can be considered as an important actuation parameter. In all three depicted geometric cases the mean averaged Nusselt number ratio is increased significantly for each investigated pulse frequency. Thereby, two significant maxima in Nusselt number enhancement for each function graph can be detected. One maximum is localized at $f = 300$ Hz independently from the depicted impingement distances. This can be explained by geometric resonance effects induced mainly by the cooling air supply lines used [24]. These additional influences of cooling air supply

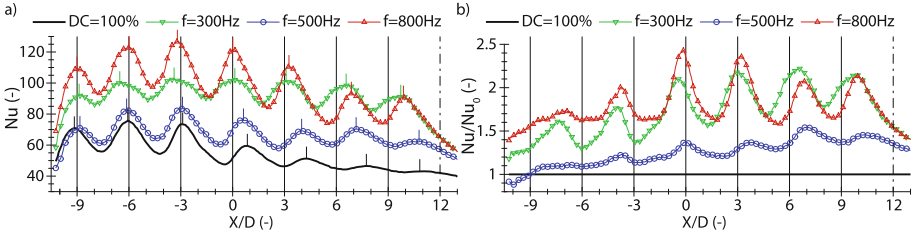


Fig. 4. Steady vs. coherent pulsed blowing ($DC_D = 50\%$, $PS = 0\%$) local convective heat transfer for flat plate configuration with $S/D = 3$ and $H/D = 3$ at $Re_D = 7000$. a) Absolute local Nusselt numbers. b) Local Nusselt number enhancements.

infrastructure are not discussed in this work, but this resonance frequency can be varied by changing the tube length before and after solenoid valves or changing the cooling air mass flow.

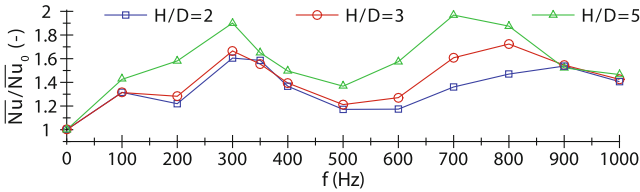


Fig. 5. Global Nusselt number ratio vs. pulse frequency with $DC_D = 50\%$ and $PS = 0\%$ for flat plate configuration with $S/D = 3$ at $Re_D = 7000$. Various impingement distances $H/D = 2$, $H/D = 3$ and $H/D = 5$.

$H/D = 5$ is the largest impingement distance investigated in this work. Thus, outflow conditions are mostly similar to free stream conditions at least close to the jet exit. The second maximum in Nusselt number enhancement for $H/D = 5$ is located at a pulse frequency of $f = 700$ Hz which can be traced back on nozzle geometry based resonance. The nozzle geometry itself has a resonance frequency at about $f = 700$ Hz which can be detected under free stream conditions without impingement plate as well [24]. Similar effects were also observed by Janetzke et al. [10, 25].

For decreasing impingement distance to $H/D = 3$ and $H/D = 2$ the second maximum in Nusselt number ratio is shifted to higher pulse frequency $f = 800$ Hz and $f = 900$ Hz under otherwise identical conditions. This can be interpreted as influence of wall distance. Based on the results presented here it is concluded that the smaller the impingement distance the higher the pulse frequency of the second maximum of Nusselt number enhancement. Furthermore, the level of Nusselt number enhancement increases with increasing impingement distance, because pulsed jets at an equivalent mean jet exit velocity are capable of transporting

their kinetic energy and momentum over a wider range before they break down and dissipate compared to their corresponding steady blowing jet.

As indicated by flow case c) depicted in Fig. 3 a reduction in convective heat transfer must be expected if pulse parameter are chosen accordingly. Although, local reductions in Nusselt number ratio was observed for pulse frequency of $f = 500$ Hz the spatially averaged value over the heated area exceed the corresponding steady blowing reference case, which is also valid for all depicted curves in Fig. 5 representing impingement distances $H/D = 2$ and $H/D = 5$.

Wall Curvature Variation: Plate curvature as a new geometric parameter was considered, which is a vital step towards investigating more realistic internal flow guidance in style of turbine blades. The flat plate configuration initially investigated serves as reference flow case.

In Fig. 6 the mean Nusselt number ratio is plotted against coherent pulse frequency with a duty cycle of $DC_D = 50\%$. In general all three graphs follow the course as it has been established for the flat plate configuration. Apart from minor deviations in convective heat transfer for almost every single pulse frequency except for $f = 200$ Hz in the convex flow case the applied radius plays a subordinate role for global actuation characteristics at least for the surface averaged Nusselt number ratio. Local maxima and minima can be detected at the same location in all three cases.

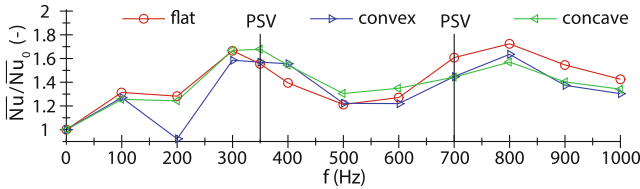


Fig. 6. Global Nusselt number ratio vs. pulse frequency for $S/D = 3$, $H/D = 3$, $DC_D = 50\%$ and $PS = 0\%$ at $Re_D = 7000$. Various target plate curvatures: flat, convex and concave.

Pulse phase shift between adjacent impingement jets has crystallised as additional time parameter for periodic heat transfer optimizations. Therefore, in Fig. 6 two frequencies were marked for phase shift variations (PSV). Figure 7a) illustrates additional significant increases in Nusselt number ratio for $f = 350$ Hz and $DC_D = 50\%$ compared to the corresponding coherently pulsed flow case at $PS = 0\%$. For the flat configuration a maximum increase of $\Delta \overline{Nu}/\overline{Nu}_0 \approx 89\%$ is achieved located at $PS = 15\%$ with a constantly high level up to $PS = 75\%$ with $\Delta \overline{Nu}/\overline{Nu}_0 \approx 87\%$. 10% and 85% pulse time shift lead to maximum Nusselt numbers for the convex case whereas maximum heat transfer is enhanced by up to $\Delta \overline{Nu}/\overline{Nu}_0 \approx 87\%$ with a constant high level in between. In case of the concave wall shape a phase shift between $30\% \leq PS \leq 70\%$ leads to a evenly high increase in heat transfer of about $\Delta \overline{Nu}/\overline{Nu}_0 \approx 80\%$ compared to the steady blowing case.

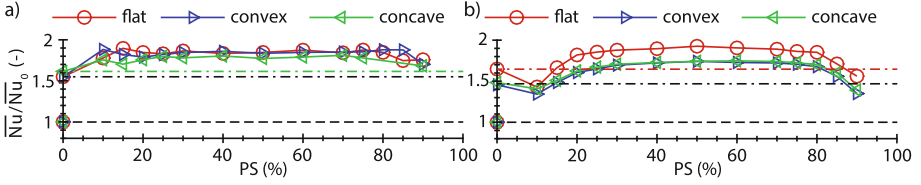


Fig. 7. Global Nusselt number ratio vs. pulse phase shift for $S/D = 3$ and $H/D = 3$ at $Re_D = 7000$. Various target plate curvatures: flat, convex and concave. a) Pulse frequency $f = 350$ Hz, $DC_D = 50\%$. b) Pulse frequency $f = 700$ Hz, $DC_D = 50\%$.

Equivalent phase shift variations were conducted for 700 Hz pulse frequency, see Fig. 7b). Between $PS = 15\%$ and $PS = 85\%$ additional significant increases in Nusselt number ratio compared to the corresponding coherently pulsed flow case at $PS = 0\%$ can be achieved. In all three geometric cases the maximum increase in convective heat transfer is located almost symmetrically at 50% phase shift which represents perfectly alternating pulsed impingement jets of adjacent nozzle rows or simultaneously pulsed jets of every second down stream nozzle row. Thereby, a Nusselt number increase of $\Delta \overline{Nu} / \overline{Nu}_0 \approx 92\%$ was achieved for the flat target plate and $\Delta \overline{Nu} / \overline{Nu}_0 \approx 74\%$ for both curved configurations.

Duty Cycle Variation: Experimental results for wall curvature variations presented in the previous paragraph have shown very similar characteristics of convective heat transfer for pulse frequency and pulse phase shift variations. It can be assumed that pulse duty cycle characteristics are also equivalent at least between the considered wall curvatures. Thus, the following discussed experimental results are focused on the convex shaped configuration.

In Fig. 8 Nusselt number ratio versus duty cycle is illustrated for a pulse frequency of $f = 350$ Hz and various nozzle Reynolds numbers up to $Re_D = 7000$. In theory, convective heat transfer is connected to temperature and velocity wall boundary layers and their development. Apart from local temperature gradients which are fundamental for heat transfer local velocity gradients on the wall are essential as well. Due to pulsations velocity wall boundary layers and their generally higher transient wall gradients are subjected to periodic renewals before they would reach steady state properties with lower wall gradients and thus lowered convective heat transfer rates. Thereby, jet momentum is a driving parameter for wall boundary layer development. Thus, it could be presumed that heat transfer enhancements are inversely proportional to duty cycle as it is theoretically valid for jet momentum expressed in Eq. 7. But an inverse, almost linear connection between Nusselt number enhancement and duty cycle is discovered in the range of $50\% \leq DC_D \leq 100\%$ and is very similar with minor deviations for all three depicted Reynolds numbers.

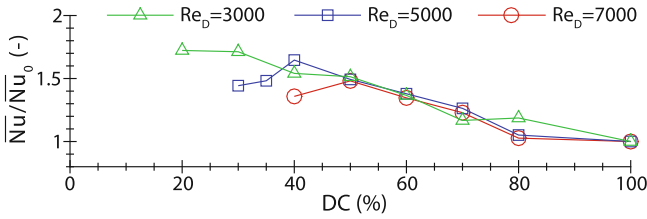


Fig. 8. Global Nusselt number ratio vs. pulse duty cycle at $f = 350$ Hz for $S/D = 3$, $H/D = 3$ and convex curved target plate. Various nozzle Reynolds numbers.

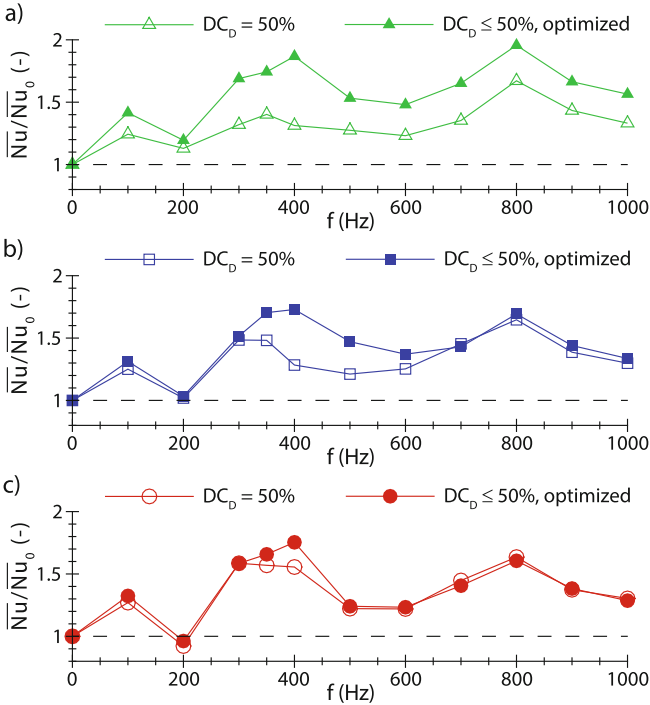


Fig. 9. Global Nusselt number ratio for coherent actuation and optimized pulse duty cycle for $S/D = 3$, $H/D = 3$ and convex curved target plate. Various nozzle Reynolds numbers: a) $Re_D = 3000$, b) $Re_D = 5000$, c) $Re_D = 7000$.

Lowering the pulse duration further to 40% or 20% of time period the inverse linear correlation is extended to higher convective heat transfer values for $Re_D = 5000$ and $Re_D = 3000$. Below specified duty cycles the increases collapse. The deviation of the temporal jet exit velocity profile from the perfect square wave signal is a result of the transmission behaviour of the pneumatic valve-nozzle actuation system. More detailed results regarding this topic are documented in [19].

In the further course optimizations regarding heat transfer enhancements based on duty cycle variations were extended. Results depicted in Fig. 8 exemplarily point out that only a reduction below $DC_D \leq 50\%$ is capable of further increasing the Nusselt number ratio. Figure 9 illustrates the achievements for the nozzle Reynolds numbers already discussed. The duty cycle of 50% is defined as reference value because it is the design point of the valves delivering a constant symmetric switching performance within the depicted frequency range. Thus, the corresponding Nusselt number curves are plotted for every Reynolds number as lower target value curve. Thereby, the largest potential in heat transfer enhancements due to duty cycle optimizations was found for the lowest investigated nozzle Reynolds number $Re_D = 3000$ within the whole frequency range of $0 < f \leq 1000$ Hz (case a)). Increasing the Reynolds number to $Re_D = 5000$ the frequency range is significantly reduced to $300 \text{ Hz} < f < 700$ Hz (case b)). Finally, the discussed frequency range is minimized to $300 \text{ Hz} < f < 500$ Hz in case c) at $Re_D = 7000$.

4 Summary and Conclusions

This work presents latest experimental results from the sub project B03 as part of the Collaborative Research Centre 1029 (SFB 1029). Thereby, the influence of periodically pulsed impingement jets arranged in a 7 by 7 inline pattern on the local and global convective heat transfer on a target plate was investigated experimentally. Regarding this topic, several investigations were performed by the authors in the recent past. This study extends the already existing database by considering primarily curvature of flow guidance as important geometrical parameter to comply step by step with realistic boundary conditions. Starting from a flat impingement plate configuration with reduced nozzle spacing of $S/D = 3$ and a fixed target plate distance of $H/D = 3$ two more curvatures, one in a convex and the other one in a concave design, were integrated in the same global experimental test setup. Convex and concave wall shapes represent internal structure of pressure side as well as of suction side of real turbine blades. Based on liquid crystal thermography measurement technique applied on a electrically heated impingement plate the local wall temperature distributions were determined. In post processing local and global Nusselt numbers were calculated representing convective heat transfer between target plate and impinging jets.

The flat target plate configuration serves as geometrical reference for variations in wall curvature. Contour plots for local Nusselt number and their ratio to corresponding steady blowing case illustrate the local convective heat transfer absolute and relative in stagnation and wall jet zones exemplarily for the flat plate configuration. Thereby, pulse frequency was defined as one main driving parameter for heat transfer enhancements. For the presented flat target plate setup a pulse frequency of $f = 300$ Hz increases the Nusselt number by up to 66% for a target plate distance of $H/D = 3$. Changing only the distance to $H/D = 5$ convective heat transfer is increased by about 90% compared to corresponding steady blowing case. A second maximum in Nusselt number ratio

was found at $f = 800$ Hz for the reference plate distance of $H/D = 3$ and was calculated to $\Delta\overline{Nu}/\overline{Nu}_0 \approx 72\%$ above steady blowing case. Furthermore, a dependency between target plate distance and pulse frequency for the second maximum Nusselt number ratio was discovered. Lowering the target plate distance to $H/D = 2$ results in a Nusselt number maximized pulse frequency of $f = 900$ Hz with an increase of $\Delta\overline{Nu}/\overline{Nu}_0 \approx 53\%$. Increasing impingement distance to $H/D = 5$ results in a maximum located at $f = 700$ Hz with an increase of $\Delta\overline{Nu}/\overline{Nu}_0 \approx 96\%$. Thereby, the local heat transfer maximisations take place mainly in the wall jet zones between adjacent impinging jets upstream the stagnation areas of steady blowing case.

For all three investigated curvatures dynamic actuation of impinging jets was performed including frequency and phase shift variations. In general the qualitative comparison of frequency depending Nusselt number ratios show equivalent results. The discussed local extreme value points are located at the same frequencies. Except for one data point for convex configuration similar enhancements in convective heat transfer can be achieved for all curvatures with satisfactorily small deviations. Results for non-coherent actuation, which is expressed by pulse time shift between adjacent jet rows, discovers further space for heat transfer optimisations. Depending on curvature additional maximum Nusselt number increases lie between $54\% \leq \Delta\overline{Nu}/\overline{Nu}_0 \leq 61\%$ coherently pulsed with $f = 350$ Hz. Phase shift optimized values are further maximized to $68\% \leq \Delta\overline{Nu}/\overline{Nu}_0 \leq 89\%$. Coherent actuation with $f = 700$ Hz leads to similar increased values in the range of $45\% \leq \Delta\overline{Nu}/\overline{Nu}_0 \leq 64\%$ which can be extended by phase shift optimisations to $74\% \leq \Delta\overline{Nu}/\overline{Nu}_0 \leq 92\%$. Thereby, pulsations with 50% phase shift is capable of delivering very high Nusselt number ratios. This phase shift represents perfectly alternating pulsations between adjacent nozzle rows which is an interesting fact for actuator development. For example, self switching actuators such as fluidic oscillators could be designed for specific operating frequencies to reduce mechanical complexity. Furthermore, based on advanced manufacturing methods this kind of actuators could be integrated in components during manufacturing process resulting in only one part.

Finally the effect of pulse duration was analysed. This parameter defines the momentum rate of the impinging jets. This interacts directly with velocity wall boundary layer and influences convective heat transfer. Thereby, the transformation behaviour between switching characteristic of the employed valves and the pulsed jets have a significant impact on resulting vortex flow structures in proximity of the jets. In general a reduction of pulse duty cycle within permissible working limits is capable of significantly increasing jet momentum at constant cooling air mass flow rate. Depending on nozzle based Reynolds number and pulse frequency the maximum Nusselt number increase can amount up to $\Delta\overline{Nu}/\overline{Nu}_0 \leq 95\%$.

The combination of the three pulse parameters frequency, duty cycle and time shift of adjacent jets creates a huge parameter space with enormous potential for optimisations in any direction but not only for heat transfer matters.

Acknowledgement. “Funded by the Deutsche Forschungsgemeinschaft (DFG, German Research Foundation) - Projektnummer 200291049 - SFB 1029”. Additionally the authors thankfully acknowledge the support of the student research assistants B.Sc. Burcu Ataseven, B.Sc. Lennart Rohlfs and B.Sc. Melik Keller during the measurement process.

References

1. Bräunling, W.J.G.: Flugzeugtriebwerke, vol. 3. Springer, Heidelberg (2009). <https://doi.org/10.1007/978-3-540-76370-3>
2. Florschuetz, L.W., Metzger, D.E., Takeuchi, D., Berry, R.: Multiple jet impingement heat transfer characteristic - experimental investigation of in-line and staggered arrays with crossflow. NASA-CR-3217. Department of Mechanical Engineering, Arizona State University, Tempe, January 1980
3. Florschuetz, L.W., Truman, C.R., Metzger, D.E.: Streamwise flow and heat transfer distributions for jet array impingement with crossflow. *J. Heat Transf.* **103**, 337–342 (1981)
4. Weigand, B., Spring, S.: Multiple jet impingement - a review. *Heat Transf. Res.* **42**(2), 101–142 (2010)
5. Xing, Y., Spring, S., Weigand, B.: Experimental and numerical investigation of heat transfer characteristics of inline and staggered arrays of impinging jets. *J. Heat Transf.* **132**, 092201/1–11 (2010)
6. Liu, T., Sullivan, J.P.: Heat transfer and flow structures in an excited circular impingement jet. *Int. J. Heat Mass Transf.* **39**, 3695–3706 (1996)
7. Vejrazka, J., Tihon, J., Marty, P., Sobolik, V.: Effect of an external excitation on the flow structure in a circular impinging jet. *Phys. Fluids* **17**, 105102 (2005)
8. Hofmann, H.M., Movileanu, D.L., Kind, M., Martin, H.: Influence of a pulsation on heat transfer and flow structure in submerged impinging jets. *Int. J. Heat Mass Transf.* **50**, 3638–3648 (2007)
9. Gharib, M., Rambod, E., Shariff, K.: A universal time scale for vortex ring formation. *J. Fluid Mech.* **360**, 121–140 (1998)
10. Janetzke, T.: Experimental investigations of flow field and heat transfer characteristics due to periodically pulsating impinging air jets. *Heat Mass Transf.* **45**, 193–206 (2008). <https://doi.org/10.1007/s00231-008-0410-8>
11. Herwig, H., Middelberg, G.: The physics of unsteady jet impingement and its heat transfer performance. *Acta Mech.* **201**, 171–184 (2008). <https://doi.org/10.1007/s00707-008-0080-0>
12. Middelberg, G., Herwig, H.: Convective heat transfer under unsteady impinging jets: the effect of the shape of the unsteadiness. *J. Heat Mass Transf.* **45**, 1519–1532 (2009). <https://doi.org/10.1007/s00231-009-0527-4>
13. Bons, J., Sondergaard, R., Rivir, R.: The fluid dynamics of LPT blade separation control using pulsed jets. *J. Turbomach.* **124**(1), 77–85 (2002)
14. Scholz, P., Ortmanns, J., Kaehler, C., Radespiel, R.: Leading edge separation control by means of pulsed jet actuators. In: 3rd AIAA Flow Control Conference, AIAA AVIATION Forum, no. AIAA 2006-2850 (2006)
15. Haucke, F.: Aktive Stroemungskontrolle zur Effizienzsteigerung von Hoch\auf\triebs\kon\fi\gu\ra\ktion\en. Ph.D. thesis, Technische Universitaet Berlin (2016)

16. Haucke, F., Nitsche, W., Peitsch, D.: Enhanced convective heat transfer due to dynamically forced impingement jet array. In: Proceedings of ASME Turbo Expo 2016, no. GT2016-57360 (2016)
17. Berthold, A., Haucke, F.: Experimental investigation of dynamically forced impingement cooling. In: Proceedings of ASME Turbo Expo 2017: Heat Transfer, ASME Turbo Expo 2017: Turbomachinery Technical Conference and Exposition, vol. 5A, no. GT2017-63140 (2017)
18. Berthold, A., Haucke, F.: Experimental study on the alteration of cooling effectivity through excitation-frequency variation within an impingement jet array with sidewall induced crossflow. In: King, R. (ed.) Active Flow and Combustion Control 2018. NNFMMMD, vol. 141, pp. 339–353. Springer, Cham (2019). https://doi.org/10.1007/978-3-319-98177-2_21
19. Berthold, A., Haucke, F., Weiss, J.: Flow field analysis of a dynamically forced impingement jet array. In: AIAA Scitech 2020 Forum, no. AIAA 2020-2081 (2020)
20. Berthold, A., Haucke, F.: Influence of excitation frequency, phase shift and duty cycle on cooling ratio in a dynamically forced impingement jet array. *J. Turbomach.* **142**(5), 051001 (2020)
21. Neumann, N., Berthold, A., Haucke, F., Peitsch, D., Stathopoulos, P.: Pulsed impingement turbine cooling and its effect on the efficiency of gas turbines with pressure gain combustion. *J. Turbomach.* **143**(7), 071016 (2021)
22. Thulin, R.D., Howe, D.C., Singer, I.D.: Energy efficient engine high pressure turbine detailed design report. Technical report, NASA CR-165608, NASA - Lewis Research Center (1982)
23. Timko, L.P.: Energy efficient engine high pressure turbine component test performance report. Technical report, NASA CR-168289, NASA - Lewis Research Center (1984)
24. Ataseven, B., Berthold, A., Haucke, F.: Influence of system resonance on a dynamically forced impinging jet. In: Proceedings of ASME Turbo Expo 2019, Poster GT2019-92266 (2019)
25. Janetzke, T.: Experimentelle Untersuchungen zur Effizienzsteigerung von Prallkühlkonfigurationen durch dynamische Ringwirbel hoher Amplitude. Ph.D. thesis, Technische Universität Berlin (2010)